Cell Reports

Supplemental Information

MiR-93 Controls Adiposity via Inhibition of *Sirt7* and *Tbx3*

Michele Cioffi, Mireia Vallespinos-Serrano, Sara M. Trabulo, Pablo Jose Fernandez-Marcos, Ashley N. Firment, Berta N. Vazquez, Catarina R. Vieira, Francesca Mulero, Juan A. Camara, Ultan P. Cronin, Manuel Perez, Joaquim Soriano, Beatriz G. Gálvez, Alvaro Castells-Garcia, Verena Haage, Deepak Raj, Diego Megias, Stephan Hahn, Lourdes Serrano, Anne Moon, Alexandra Aicher, and Christopher Heeschen,

Figure S1 – Enhanced adiposity and adipogenesis in miR-25-93-106b$^{-/-}$ mice, Related to Figure 1.

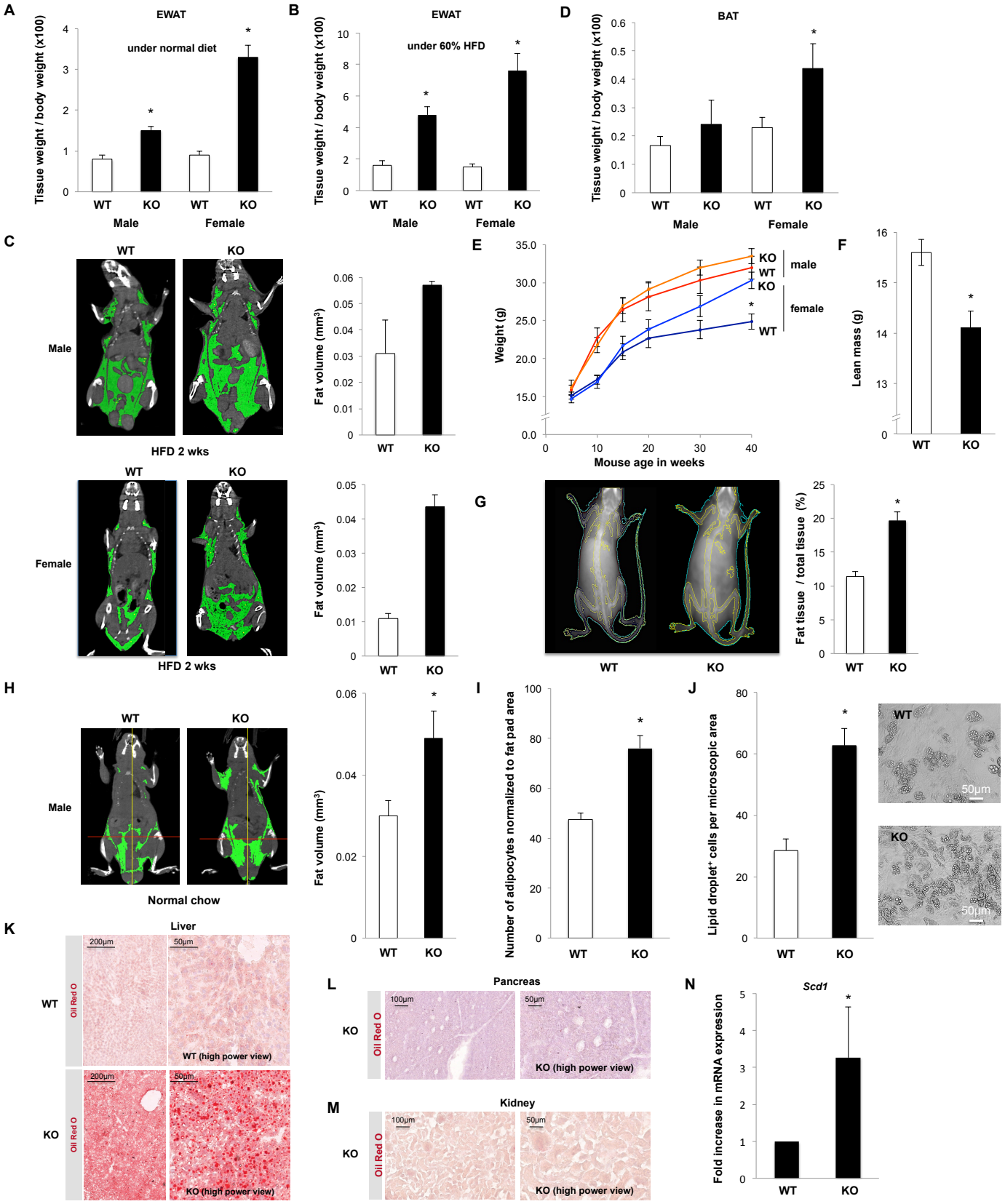

(**A**) Quantification of visceral fat pads per body weight in female and male WT and miR-25-93-106b$^{-/-}$ (KO) mice under normal chow diet (n=5, * p<0.05). **(B)** Quantification of visceral fat pads per body weight in female and male WT and KO mice under 60 % high fat diet (HFD) for 2 weeks (n=5, * p<0.05). (**C**) Computed tomography of WT versus KO mice to visualize adipose tissue. Green label indicates total fat (n=8-9, * p<0.05). **Upper**: male mice following HFD for 2 weeks; representative images and quantification. **Lower:** female mice following HFD for 2 weeks, representative images and quantification. **(D)** Quantification of BAT per body weight in female and male WT and KO mice under normal chow diet (n=5, * p<0.05). (**E**) Body weight up to 40 weeks in female and male WT and KO mice (n=4 mice per group/time point, * p<0.05). **(F)** Lean mass in WT versus KO mice (n=8, * p<0.05). **(G)** Percentage of fat tissue in female WT and KO mice (n=8-10, * p<0.05) as determined by densitometry. Representative densitometric imaging is shown (**left**), quantification **(right**). (**H**) Computed tomography of male WT and KO mice under chow diet. Green label indicates total fat (n=8-9, * p<0.05); representative images (**left**), quantification (**right**). **(I)** Number of adipocytes in KO vs. WT mice analyzed per 40x magnification picture in n=15 pictures and normalized to total fat pad size. (**J**) *In vitro* fat differentiation of sorted early adipocyte precursors from KO and WT mice. Quantitative analysis of lipid droplets following 8 days of differentiation (n=6, * p<0.05). Cryosections of liver (**K**), pancreas (**L**), and kidney (**M**) from WT and KO mice are shown (Oil Red O staining, nuclear stain in blue). Expression of *Scd1* in the liver (**N**) of KO versus WT mice (n=4, p<0.05) was used as a substitute marker to quantify fat accumulation.

Figure S2 – Molecular characterization of adipose tissue in miR-25-93-106b$^{-/-}$ mice, Related to Figure 1.

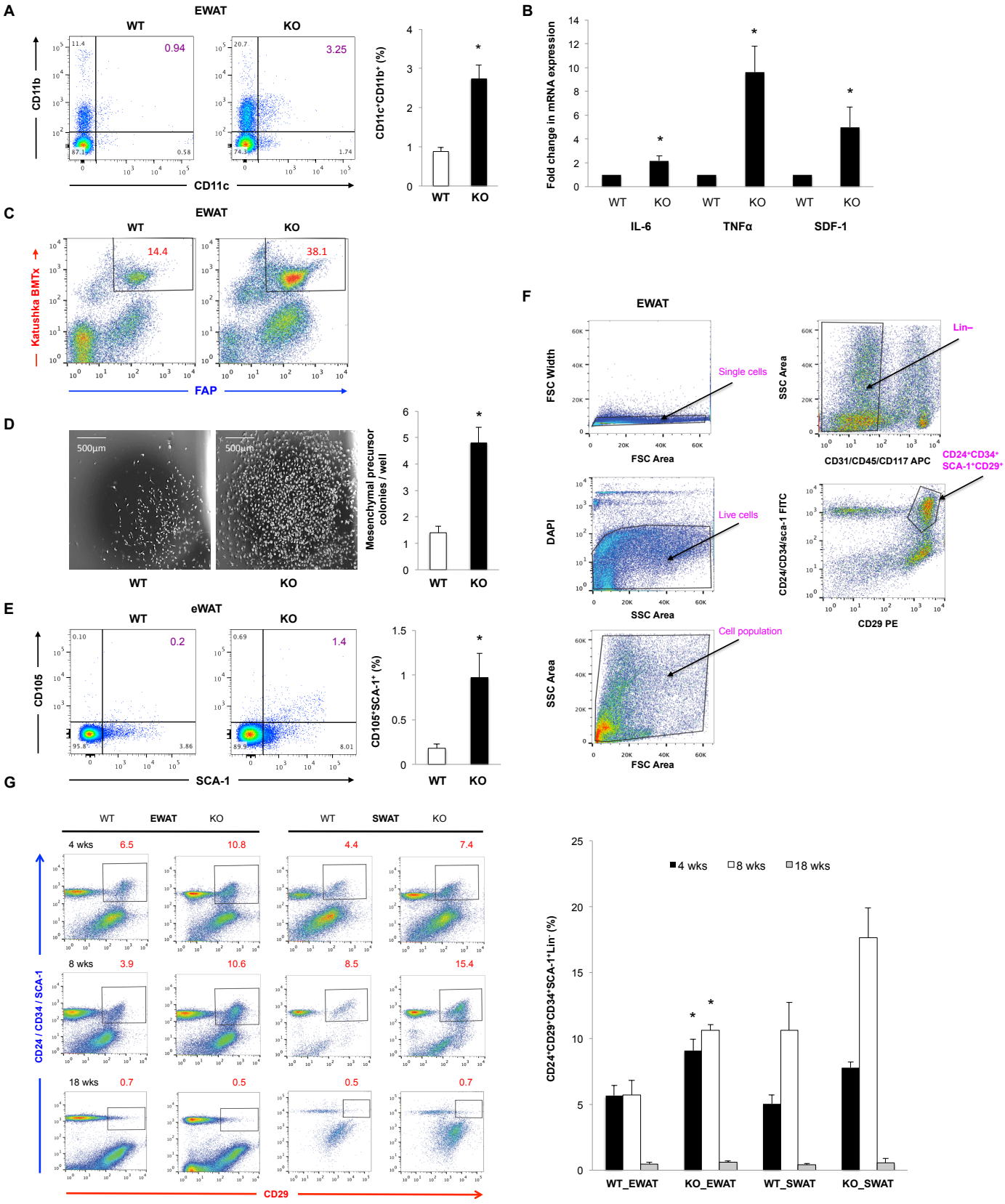

(A) Number of CD11b^{+}CD11c^{+} macrophages in the stromal vascular fraction (SVF; **left**). Quantification (n=3 mice, * p<0.05, **right**). **(B)** Relative expression of IL-6, TNFα, and SDF-1 measured by quantitative real-time PCR (n=5 mice, * p<0.05). (**C**) Bone marrow-derived FAP^{+} stromal cells in the visceral fat of miR-25-93-106b$^{-/-}$ compared with WT littermates. We performed bone marrow transplantations using bone marrow cells from transgenic mice ubiquitously expressing the far-red fluorescent protein Katushka to track bone marrow-derived cells in WT and miR-25-93-106b$^{-/-}$ recipient mice. Dual staining with the stromal cell marker fibroblast activation protein (FAP) indicates a higher percentage of bone marrow-derived (Katushka^{+}) FAP^{+} cells in the visceral fad pads from miR-25-93-106b$^{-/-}$ mice. Bone marrow-derived stromal cells have been involved in promoting adipogenesis *in vivo* and might be attracted by the enhanced production of chemokines such as SDF-1 in the visceral fat pads of miR-25-93-106b$^{-/-}$ mice. **(D)** Number of mesenchymal precursor colonies (**left**). Quantification (n=3 mice, * p<0.05, **right**). (**E**) Number of CD105^{+}SCA-1^{+} mesenchymal precursors (**left**). Quantification (n=3 mice, * p<0.05, **right**). (**F**) Representative flow cytometric gating strategy to isolate early adipocyte precursors. (**G**) Decline of early adipocyte precursors with increasing age. **Left**: representative flow cytometry. **Right**: quantification (n=3, * p<0.05). Differences in early adipocyte precursors between WT and miR-25-93-106b$^{-/-}$ (KO) mice were visible at 4 and 8 weeks of age. However, both WT and KO mice beyond an age of 8 weeks lost their adipocyte precursors and differences between WT and KO disappeared.

Figure S3 – Expression of individual miRs of the miR-25-93-106b cluster in various tissues, Related to Figure 2.

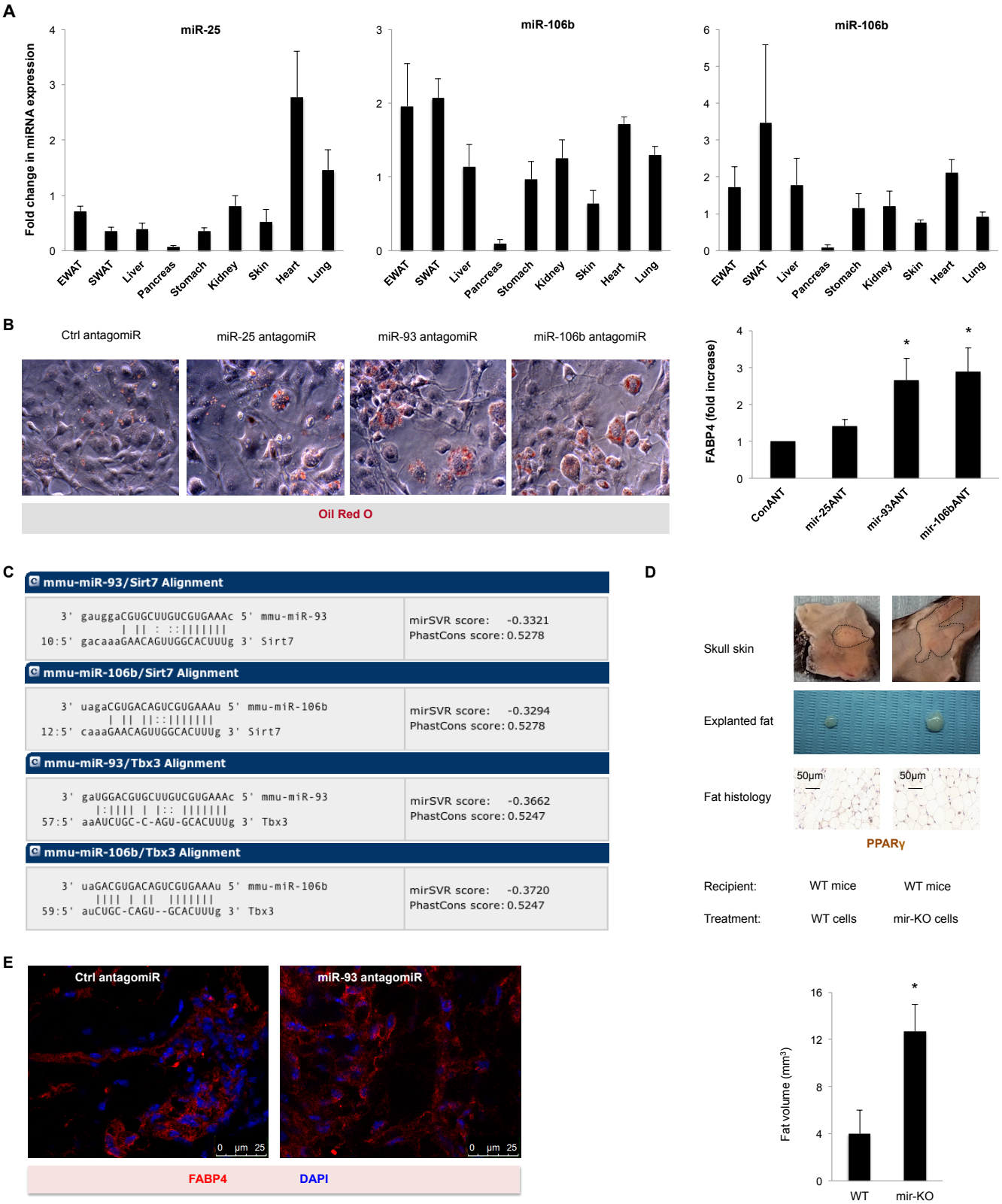

(**A**) Expression of (**left**) miR-25, (**middle**) miR-93, and (**right**) miR-106b in different organs was normalized to spleen. Female 8 week-old WT mice were used for analysis (n=3). **(B)** 3T3-L1 pre-adipocytes were kept in differentiating medium for 3 days with miR-25, miR-93, and miR-106b antagomiRs or control antagomiRs; representative images (**left**), quantification (**right**). (**C**) Mmu-miR-93 and mmu-miR-106b alignment for *Tbx3* and *Sirt7* obtained from *in silico* target prediction using www.microRNA.org. (**D**) Subcutaneous injection of sorted WT and miR-KO-derived early adipocyte precursors into the skull of WT recipients. Gross morphology *in situ* and after explantation of subcutaneously grown adipose tissue (**first two rows**). Histological analysis of adipose tissue for PPARγ expression (**middle**). Quantification of the fat volume (n=3, * p<0.05; **lower**). (**E**) Immunostaining for FABP4 / DAPI to detect cells of adipocyte lineage.

Figure S4 – *In vitro and vivo* role for *Tbx3* and *Sirt7* in adiposity, Related to Figure 3&4.

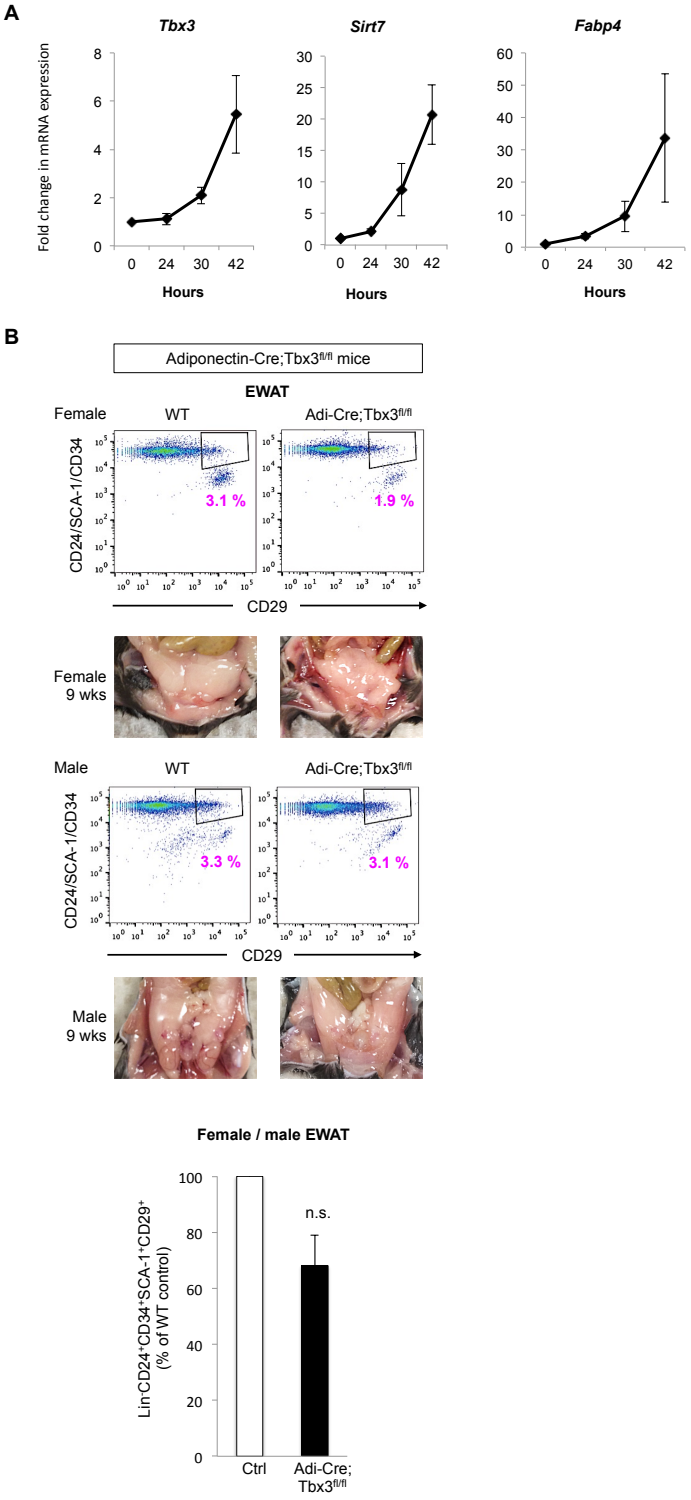

(**A**) *Tbx3* and *Sirt7* are induced early during adipocyte differentiation. As a reference *Fabp4* mRNA levels are measured. 3T3-L1 pre-adipocytes were kept in differentiating medium for up to 42h. (**B**) Representative flow cytometry of early adipocyte precursors from the EWAT of adult female and male Tbx3 adiponectin-Cre mutants vs. control (**upper**); representative images of EWAT in situ **(lower**). Quantification of early adipocyte precursors in female and male EWAT (**bottom**; n=6-8, p=n.s.).

Figure S5 – Expression of miR-25, 93, and 106b in female and male WT mice, Related to Figure 5.

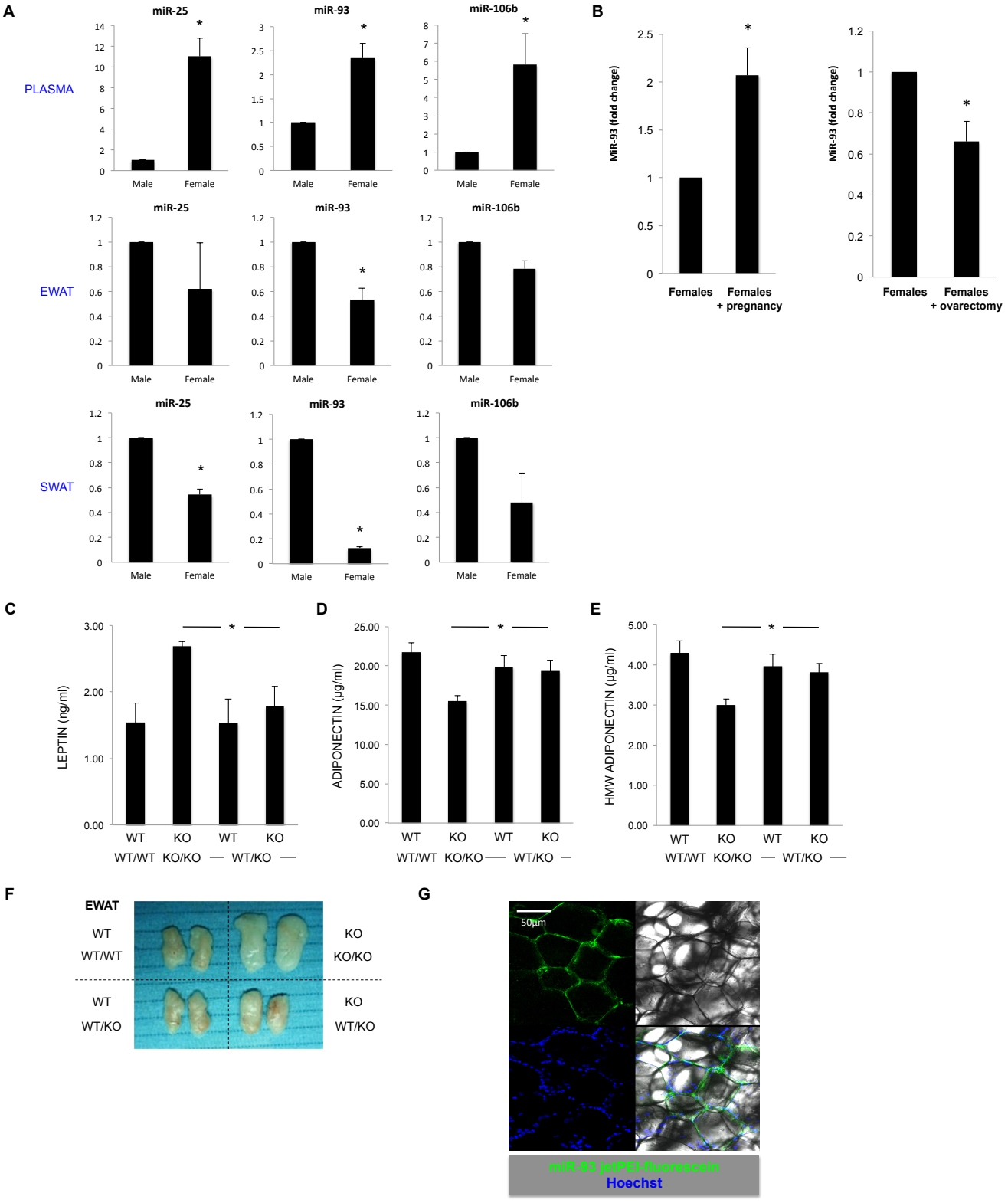

Expression of miR-25, 93, and 106b is measured in the plasma (**upper**), EWAT (**middle**), and SWAT (**lower**) of female and male WT mice (n=4, * p<0.05). (**B**) To increase estrogen levels, female 8 weeks old WT mice were mated. Plug-positive females were separated and used for experiments at gestational day 20 and compared with non-pregnant littermates. To decrease estrogen levels, female 5 weeks old mice underwent ovarectomy and were sacrificed 4 weeks after the induction of ovarectomy. MiR-93 was assessed in EWAT. (**C**) LEPTIN levels in the blood plasma of parabiotic miR-KO and WT mice (n=4 per group, * p<0.05). WT/WT=WT individual from WT/WT parabiotic couple; KO/KO=miR-KO individual from miR-KO/miR-KO parabiotic couple; KO from WT/KO: miR-KO individual from miR-KO/WT mixed parabiotic couple; WT from WT/KO: WT individual from WT/miR-KO mixed parabiotic couple. (**D**) ADIPONECTIN and (**E**) HMW ADIPONECTIN levels (n=4 per group, * p<0.05). (**F**) Representative images of EWATs from WT mice (from WT/WT pair) and KO mice (from KO/KO pair; **upper row**) and respective EWATs from mixed parabiotic WT/KO pairs (**lower row**). (**G**) Forty-eight hours following injection of miR-93 mimic jetPEI fluorescein, fresh unfixed visceral adipose tissue was placed between two glass slides for confocal analysis. Nuclei were counterstained with Hoechst. The miR-93 jetPEI fluorescein was distributed in the intercellular space between mature adipocytes, in which stromal, vascular, and precursor cells are located.

Table S1 – miRNA array in total visceral fat of ob/ob versus WT mice, Related to Figure 2.

mmu-miR-193*	up	16.72433
mmu-miR-342-3p	down	16.469057
mmu-miR-221	down	10.808439
mmu-miR-222	down	8.718003
mmu-miR-193b	up	7.929523
mmu-miR-30c-2*	up	6.4602685
mmu-miR-34c	down	6.192575
mmu-miR-193	up	4.6879935
mmu-miR-142-3p	down	4.6398153
mmu-miR-378*	up	4.6214724
mmu-miR-146a	down	4.6188216
mmu-miR-24-1*	down	4.472841
mmu-miR-30a*	up	4.4478707
mmu-miR-34b-5p	down	4.442916
mmu-miR-27b	down	4.3809237
mmu-miR-142-5p	down	4.173798
mmu-miR-378	up	3.8732448
mmu-miR-30a	up	3.6269217
mmu-miR-155	down	3.569376
mmu-miR-23b	down	3.5135841
mmu-miR-365	up	3.4014065
mmu-miR-674*	down	3.26676
mmu-miR-18a	down	3.068415
mmu-miR-203	up	3.0215619
mmu-miR-223	down	2.966157
mmu-miR-340-5p	down	2.9633613
mmu-miR-345-5p	up	2.953659
mmu-miR-145	up	2.8846698
mmu-miR-21*	down	2.8095095
mmu-miR-214	down	2.7860937
mmu-miR-204	up	2.7849007
mmu-miR-2140	up	2.757046
mmu-miR-30c	up	2.631333
mmu-miR-199a-5p	down	2.5853188
mmu-miR-30e*	up	2.5833218
mmu-miR-199a-3p	down	2.5739043
mmu-miR-376a	down	2.5723896
mmu-miR-21	down	2.5705495
mmu-miR-434-3p	down	2.5674825
mmu-miR-379	down	2.527721
mmu-miR-210	up	2.5143757
mmu-miR-1187	up	2.5114021
mmu-miR-676	up	2.497769
mmu-miR-24	down	2.4692557
mmu-miR-15b	down	2.4110744
mmu-miR-101b	up	2.3309216
mmu-miR-130a	up	2.2674763
mmu-miR-326	down	2.1619751
mmu-miR-411	down	2.1534023
mmu-miR-146b	down	2.1510344
mmu-miR-320	up	2.101649
mmu-miR-181c	down	2.0714946
mmu-miR-652	down	2.0568814
mmu-miR-136	down	2.0114508
mmu-miR-143	up	2.0053709
mmu-miR-103	up	1.9942652
mmu-miR-132	down	1.8736306
mmu-miR-16	down	1.8668082
mmu-miR-2141	up	1.8566122
mmu-miR-107	up	1.8492423
mmu-miR-1892	up	1.8454256
mmu-miR-126-5p	up	1.831872
mmu-miR-329	down	1.8278712
mmu-miR-219	up	1.7084188
mmu-miR-15a	down	1.7003222
mmu-miR-1897-5p	up	1.6990037
mmu-miR-24-2*	down	1.6897979
mmu-miR-362-3p	down	1.6644119
mmu-miR-324-5p	down	1.6470712
mmu-miR-150	up	1.6398381
mmu-let-7i	down	1.634022
mmu-miR-140	down	1.6225277
mmu-let-7b	up	1.6019388
mmu-miR-125a-5p	up	1.5997282
mmu-miR-199b*	down	1.5967468
mmu-miR-93	**up**	**1.5950526**
mmu-miR-19a	down	1.5751393
mmu-miR-7a	down	1.564266
mmu-miR-574-5p	up	1.5520502
mmu-miR-23a	down	1.5494937
mmu-miR-2137	up	1.5484319
mmu-miR-218	up	1.5371854
mmu-miR-127	down	1.5346599
mmu-miR-712	up	1.5339874
mmu-miR-29c*	up	1.5292578
mmu-miR-148a	up	1.5134623
mmu-miR-532-5p	down	1.4935311
mmu-miR-152	up	1.4917545
mmu-miR-10b	up	1.4891328
mmu-miR-30e	up	1.4860519
mmu-miR-126-3p	up	1.4821357
mmu-miR-17*	down	1.4775497
mmu-miR-151-5p	up	1.4727404
mmu-miR-128	down	1.4674917
mmu-miR-450a-5p	up	1.4646745

Given is the fold change for 28-week old male mice. Only data for changes ≥ 1.5 fold are provided.

Up: up-regulated in WT = down-regulated in *ob/ob* mice.
Down: down-regulated in WT = up-regulated in *ob/ob* mice

2. SUPPLEMENTAL MATERIAL & METHODS

Animal studies. Studies were performed with miR-25-93-106b$^{-/-}$ mice and their littermates on C57BL/6J background (kind gift of Andrea Ventura) and *ob/ob* mice from The Jackson Laboratories (Bar Harbor, ME). To generate Tbx3 KO mutants in the different adipose tissue compartments, we generated mutant mice with specific Tbx3 ablation in mature adipocytes using adiponectin-Cre mice and PDGFRa-Cre mice to generate mutant mice with Tbx3 ablation in early adipocyte precursors, SVF, and mature adipocytes (Berry and Rodeheffer, 2013). Thus, Adiponectin-Cre and PDGFRa-Cre mice were bred to Tbx3Dflox/Dflox mice (Frank et al., 2012). Sirt7KO mice and their littermates were provided by Lourdes Serrano, Rutgers University, Piscataway, NJ.

Adipoq^{Cre} (stock # 010803) and *Pdgfra*^{Cre} (stock# 013148) bearing mice were obtained from Jackson labs. Each line was bred to a *Tbx3*$^{flox/flox}$ homozygote (allele described in Frank et al., 2012 and Frank et al 2013) and male progeny with the genotype of *Tbx3*$^{flox/+}$*; Pdgfra*$^{Cre/+}$ or *Tbx3*$^{flox/+}$*; Adipo*$^{Cre/+}$ were used for generating mutant and control embryos and fetuses by breeding to *Tbx3*$^{flox/flox}$ females. The *Tbx3*$^{flox/flox}$ mice are in a mixed background of C57Bl6/Sv129/FvbNJ. For some experiments, pregnant mice were studied at gestational day 20. Age and gender-matched mice were fed either control chow diet or high-fat diet (60%) (D12492 from Research Diets, Inc.).

All animal procedures were conducted in compliance to the 3Rs and were approved by the Institute's Institutional Animal Care and Use Committee (CBA 68_2013 & CBA 25_2009 & PPL70-8129). Mice were housed in standard 12-hour light / dark conditions with *ad libitum* access to food and water. All surgeries were performed using aseptic techniques and under general anesthesia using 5% isoflurane for induction and about 3% isoflurane for maintenance. Animals were pre-medicated with a subcutaneous injection of 0.05mg/kg of buprenorphine (Schering-Plough). Meloxicam (Boehringer Ingelheim; 0.3mg/kg) once daily was subcutaneously injected to minimize postoperative pain for up to three days. If not stated otherwise, we used female mice aged 6-12 weeks for our experiments with miR-25-93-106b$^{-/-}$ mice. Only for metabolic assays and imaging purposes (glucose, insulin, oxylet measurements, densitometry, and computed tomograpghy) mice aged 13-25 weeks were used. Moreover, we used 5-7

week-old *ob/ob* mice if not stated otherwise.

Indirect calorimetry. We performed indirect calorimetry using Oxylet System metabolic chambers (Panlab Harvard Apparatus). Acclimatization of mice to the measurement cages was three days prior to data recording. Room temperature was constantly kept at 21°C, while running light/dark cycles of 12h. Respiratory Quotient (RQ) was calculated as RQ=VCO2/VO2 from volumes of consumed O2 (VO2) and eliminated CO2 (VCO2) recorded every 24min. We calculated Energy Expenditure (EE) as EE= (3.815+(1.232xRQ)) x VO2 x 1.44). Moreover, we recorded food intake and rearing activities (defined as standing upright) in time intervals of 20min during the whole measurement period.

Bone marrow transplantations. Bone marrow transplantations in miR-25-93-106b KO mice and their littermates were performed as previously described (Aicher and Heeschen, 2007; Aicher et al., 2007). Briefly, miR-25-93-106b KO mice (about 5 weeks old) were irradiated with 12 Gy. Twenty-four hours later, bone marrow from miR-25-93-106b KO mice and their WT littermates was intravenously injected. To assess the transplantation efficiency, bone marrow from mice constitutively expressing the far-red fluorescent protein Katushka (a kind gift of Sagrario Ortega) were used. Mice were kept under oral treatment with enrofloxacine (Baytril 2.5%, Bayer) with 1ml/100 ml drinking water to prevent infections. Bone marrow reconstitution was allowed to take place and mice were used for experiments 6 weeks after the bone marrow transplantation.

Ovarectomy. Ovarectomy was performed according to (Armamento-Villareal et al., 2005). Briefly, ovariectomy or sham operation was performed in 5 week-old females. Ovaries were exposed through an abdominal approach and resected using an electrocoagulator, followed by suturing of muscles and skin of the abdomen. Mice were sacrificed 4 weeks after induction of ovarectomy.

Computed tomography. For computer tomography (CT), mice were anesthetized with a continuous flow of 1–3% isoflurane/oxygen mixture (2l/min), and scanned using a eXplore Vista PET-CT (GE Healthcare). Images of the whole body were analyzed with MMWS/Vista software. Regions of interest (ROI) were created growing a seed with the same density of fat tissue to quantify the volume of fat.

Dual-energy X-ray absorptiometry (DEXA). Scans were made by PIXImus scans (PIXImus, LUNAR,

Madison, WI), which provide skeletal and body composition data such as fat mass (g), and % fat mass. The PIXImus small animal densitometer (DEXA) has a resolution of 0.18x0.18 mm pixels and is equipped with software version 1.46.

ELISAs. Peripheral blood plasma samples were obtained using EDTA vials, followed by centrifugation at 3000 rpm for 10 min at 4ºC. The obtained plasma was stored at -80ºC prior to use. To assess insulin and adiponectin levels, an ultrasensitive mouse insulin ELISA (Mercodia, 10-1249-01), mouse adiponectin ELISA kit (Abcam, ab108785), and total and high molecular weight (HMW) adiponectin ELISA (ALPCO, 47-ADPMS-E01) were used according to manufacturer's instructions.

Analysis and sorting of adipocyte precursors. Adipose tissue was mechanically homogenized using scalpels, incubated with collagenase P (Roche; 1mg/ml) for 20 min at 37 °C, and filtered through 40µm cell strainers to obtain the stromal vascular fraction prior to staining with anti-mouse CD31-APC, CD45-APC, CD117-APC (1:50 in PBS; BD Biosciences) for depletion, followed by CD24-FITC (1:50 in PBS; ebiosciences), SCA-1-FITC, CD34-FITC, and CD29-PE (1:50 in PBS; eBiosciences) for 10 min at room temperature. Live cells negative for 4',6-Diamidino-2-phenylindol (DAPI; Sigma: 1 mg/ml) were then analyzed and sorted using a BD influx or ARIA II cell sorter.

Alternatively, e.g. if GFP^+ cells were involved, staining with CD31-Pacific Blue, CD45-Pacific Blue, and CD117-Pacific Blue (all 1:50 in PBS; Biolegend) for depletion, followed by CD24-Alexa Fluor 647, SCA-1-Alexa Fluor 647, CD34-Alexa Fluor 647 (all 1:50 in PBS; Biolegend), and CD29-PE (1:50 in PBS; eBiosciences) for 10 min at room temperature. Live cells negative for 7-aminoactinomycin D (7-AAD; Sigma: 20 mg/ml) were then analyzed.

In case that platelet-derived growth factor receptor a (PDGFR a; CD140a)-Cre Tbx3 ablation mutants were used, additional staining with CD140a-PECy7 (1:50 in PBS; eBiosciences) was included. In this setup, SCA-1 was separately stained using SCA-1-Alexa Fluor 700 (1:50 in PBS; eBiosciences). For some experiments, we also identified mesenchymal precursors by staining with CD105-PE (1:50 in PBS; ebiosciences) and SCA-APC (1:50 in PBS; ebiosciences). Equal amounts of $CD105^+$ $SCA\text{-}1^+$ cells were sorted and seeded into collagen-coated 96 wells. After two weeks, mesenchymal

colonies had formed and were scored. Moreover, pro-inflammatory cells were identified by staining for CD11b-FITC (1:50 in PBS; BD Biosciences) and CD11c-APC (1:50 in PBS; BD Biosciences) for 30min at 4ºC. Live cells negative for DAPI were then measured using a BD FACSCanto II or Fortessa cell analyzer. From this protocol, we also obtained mature adipocytes as floating fraction after pelleting the stromal vascular fraction.

Cell cycle analysis using DAPI. Cells were centrifuged, washed with cold PBS, and resuspended in 300ml of PBS, while 700ml ice-cold 100% ethanol were added drop by drop on a vortex. After leaving on -20°C overnight, cells were washed twice with cold PBS, resuspended, and incubated in 1 mg/ml DAPI for at least 2 hours at 4°C. Cell cycle analysis was performed using the Dean-Jett-Fox model of the FlowJo version 9.5.2.

Cell culture and adipocyte differentiation. For differentiation into adipocytes, we used sorted $CD24^{+}CD29^{+}SCA\text{-}1^{+}CD34^{+}CD31^{-}CD45^{-}CD117^{-}$ adipocyte precursors of the visceral fad pad or subcutaneous fat. Cells were first cultured on collagen-coated 96-well plates in Dulbecco's modified Eagle medium (DMEM) with 10% fetal calf serum (FCS), 100I.U./ml penicillin, 100mg/ml streptomycin, and 2mM L-glutamine (complete medium) to obtain primary murine pre-adipocytes. When using embryonic cells, isolated early adipocyte precursors from E16.5 to E18.5 were cultured on collagen-coated wells as mouse embryonic fibroblasts (MEF).

Moreover, primary human pre-adipocytes from subcutaneous adipose tissue were purchased from Zenbio and maintained with human Pre-adipocyte Medium (Zenbio; PM-1). In addition, we used murine 3T3-L1 pre-adipocytes (Zenbio) that were maintained in complete DMEM containing 25mM glucose. For differentiation, cells were plated at high density (80% confluency). After reaching 100% confluency 48 hours later, medium was changed to DMEM supplemented with 10% FCS with 1µM dexamethasone (Sigma), 0.5mM isobutylmethylxanthine (IBMX; Sigma), 100µM indomethacin (Sigma), and 1µg/ml insulin (Sigma) for the indicated time points. For primary cells, we additionally added 10µM rosiglitazone (Cayman Chemical) or used commercially available differentiation medium (Zenbio: OM-

DM). Following two days in differentiation medium, cells were maintained by complete DMEM with 1µg/ml insulin.

Apart from induced fat differentiation, 3T3-L1 preadipocytes also show spontaneous differentiation over a period of several weeks into adipocytes when cultured with fetal calf serum (Gregoire et al., 1998). We observed spontaneous differentiation starting from two weeks after reaching 100% confluency and scored the number of lipid droplet-containing adipocytes. After differentiation into adipocytes, cells were fixed in 10% formaldehyde in PBS for 15min, and subsequently incubated with Oil Red O (Sigma; stock solution: 0.5% Oil Red O (w/v) in isopropanol) working solution (60% (v/v) Oil Red O stock solution in deionized water) for 60min. Staining solution was removed by washing with deionized water.

Flow cytometry of lipid droplet-containing adipocytes. Following induction of *in vitro* fat differentiation, lipid droplet-containing cells were identified by LipidTOX staining (LipidTOX green or far red; Lifetechnologies) diluted 1:1000 in PBS for 10 min at room temperature. Live cells negative for DAPI were then analyzed by flow cytometry.

Analysis of adipocyte size and number. The automated Adiposoft software was used for the analysis of white adipose tissue cell size and number, as described in (Galarraga et al., 2012).

In vitro and in vivo experiments using miRNA inhibitors/mimics. Inhibition of miR-93 *in vitro* was achieved by administering mmu-miR-93 antagomirs or scrambled control at 1.2µM (Biospring, Frankfurt, Germany) for the indicated time points.

Control_antagomir (sequence 5' → 3')	A*A*G *C*AC GCG CGU UGA GA*A *U*U*G
MiR-93 antagomir (sequence 5' → 3')	C*U*A CCU GCA CGA ACA GCA C*U*U *U*G
MiR-106b antagomir (sequence 5' → 3')	A*U*C UGC ACU GUC AGC AC*U *U*U*A

5' modifications: in some experiments we used antagomirs labeled with Cy3 (Cyanine 550)

3' modifications: Cholesterol

all nucleotides = 2'-O-Methyl nucleotides and * = phoshorothiates

To study the effect of mir-93 inhibition in freshly sorted early adipocyte precursors from visceral adipose tissue, sorted cells were incubated with mir-93 antagomiRs or control antagomiRs for 60 min at 37ºC prior to injection in an equal volume (50µl) of Matrigel^{TM} (BD Biosciences) into the fat-free occipital skull region of female nude mice (Foxn1nu, Charles River Laboratories) to assess *in vivo* growth.

Overexpression of miR-93 *in vitro* was performed using either miR-93 mimics versus controls (Sigma) or lentiviral miR-93 carrying eGFP as a reporter versus scrambeled control (Genecopoeia). Replication-incompetent lentiviral particles were produced by calcium-phosphate transfection of HEK293T cells using the packaging plasmids pMD.2G (VSV-G) and pPAX2, and either miR-93 or miR-93 control plasmids as shuttle vectors. The medium was replaced for fresh DMEM medium with 10% FCS and antibiotics 6h after transfection, and 48h afterwards the medium was collected, cleared by low-speed centrifugation, filtered through 0.45µm pore-size PVDF filters, and stored in aliquots at -80ºC.

We also transduced 3T3-L1 with lentiviral miR-93 and controls. Cells were sorted for GFP expression and used for experiments.

In addition, we transduced miR-KO bone marrow mesenchymal stem cells (MSC) with lentiviral miR-93 and controls. Bone marrow MSCs were obtained by crushing and flushing tibia bones from miR-KO mice. Cells were first cultured on collagen-coated 24 wells. After 24 hours, we used the non-adherent fraction, while adherent cells were discarded. The non-adherent cells were further expanded and used for experiments after depletion of remaining $CD45^+$ cells by flow cytometry.

Overexpression of miR-93 *in vivo*: Mice received injections of miR-93 mimics administered in a liposomal formulation (*in vivo* jet-PEI-FITC from Polyplus transfection, see **Fig. S14**). PEI–based cationic polymer, in vivo-jet-PEI-FITC, was used for the in vivo delivery of miR-93 mimics according to the manufacturer's instructions. Per injection into one fad pad, we diluted 20 µg of siRNA and 3 µl of in vivo-jet PEI in endotoxin-free 5% (w/v) glucose separately and then mixed together to give an N:P ratio of 7.5:1 in a final volume of 100µl. Injections were repeated after two weeks, and mice were sacrificed 4 weeks after the first injections. To perform intravisceral fat pad injections, abdominal incisions were made and the miR mimics were carefully distributed. Following externalization, the fat pads underwent

digital caliper measurements. Fat volume was calculated by the modified ellipsoidal volume: (length x width x height) x ½ (Tomayko and Reynolds, 1989).

Quantitative real-time polymerase chain reaction (qPCR). Total RNA was isolated using QIAzol (Qiagen) according to the manufacturer's instructions. For analysis of miRNA from peripheral blood, we collected whole peripheral blood into EDTA-containing tubes, and allowed the samples to stand for 10 min at RT. Separation of plasma was accomplished by centrifugation at 3000 rpm for 10min at 4ºC. The plasma obtained was then transferred into new tubes, and 200µl plasma were mixed with 800µl QIAzol solution. To isolate RNA from whole adipose tissue, we homogenized the fat pads (about 0.02 g/800µl QIAizol) using a gentleMACS dissociator (Miltenyi Biotec), and permitted complete dissociation of nucleocomplexes and separation of the lipid layer by incubation for 15min at 30ºC. After removal of the lipid layer, samples underwent the standard QIAzol protocol according to the manufacturer's instructions. Complementary DNA for miRNA qPCR was synthesized using the NCode VILO miRNA cDNA synthesis kit (Invitrogen). qPCR was performed using Express SYBR GreenER Supermix with premixed ROX (Invitrogen). Ct values were normalized to housekeeping genes such as SNORD95 (ΔCt), and relative expression was calculated using the $2^{-\Delta\Delta Ct}$ method. Primers for miRNA qPCR for miR-25, miR-93, miR-106b, and SNORD95 were purchased from Qiagen.

Complementary DNA for non-miRNA qPCR from sorted cells was synthesized using the SuperScript VILO cDNA synthesis kit (Invitrogen). To increase yields of complementary DNA, transcription was performed for 2 hours at 42ºC. Complementary DNA for non-miRNA qPCR from total tissues and unsorted cells was synthesized using the QuantiTect Reverse Transcription kit (Qiagen). qPCR was performed using PerfeCTa SYBR Green fastMix low Rox (Quanta Biosciences). Ct values were normalized to housekeeping genes such as HPRT or 18s rRNA (ΔCt), and relative expression was calculated using the $2^{-\Delta\Delta Ct}$ method.

List of utilized primers

m18S RNA	forward 5'GCAATTATTCCCCATGAACG 3' reverse 5'GGCCTCACTAAACCATCCAA 3'
mHPRT	forward 5'TCCTCCTCAGACCGCTTTT 3' reverse 5'CCTGGTTCATCATCGCTAATC 3'
mSirt7	forward 5'TGTGGACACTGCTTCAGAAAGGGA 3' reverse 5'CACAGTTCTGAGACACCACATGCT 3'
mTbx3	forward 5'AGGAGCGTGTCTGTCAGGTT 3' reverse 5'GCCATTACCTCCCCAATTTT 3'
mPDGFRa	forward 5'AACGGAGGAGCTGCGGGGAA 3' reverse 5'CCCATAGCTCCTGAGACCTTCTCCT3'
mCD24	forward 5'ACGGAGCGGACATGGGCAGA 3' reverse 5'TTGGTTGCAGTAAATCTGCGTGGGT3'
mFABP4	forward 5'GATGAAATCACCGCAGACGACA 3' reverse 5'ATTGTGGTCGACTTTCCATCCC3'
mTNFa	forward 5'GCCTCTTCTCATTCCTGCTTG3' reverse 5'CTGATGAGAGGGAGGCCATT3'
mIL-6	forward 5'GACAACTTTGGCATTCTGG3' reverse 5'ATGCAGGGATGATGATGTTCTG3'
mCxcl12 (mSDF-1)	forward 5'GAAAGCTTTAAACAAGAGGCTCAA3' reverse 5'CTATGGGCCCTTCCCTAACAC 3'
mScd1	forward 5'CAGGTTTCCAAGCGCAGTTC3' reverse 5'ACTGGAGATCTCTTGGAGCA3'

For the quantification of *Nanog*, *Tbx3*, *Oct4*, and *Sox2*, TaqMan probes were run according to the manufacturer's protocol using Taqman Universal PCR MasterMix, No AmpErase, UNG (Applied Biosystems). Ct values were normalized to 18S rRNA or HPRT.

miRNA expression analyses and data processing. Total RNAs isolated from male ob/ob mice (n=4 of either group; 28 weeks old) were hybridized to the mouse microRNA Microarray (G4471A Mouse AMADID 029152, miRNA Sanger V15, Agilent Technologies). MicroRNA labeling, hybridization and washing were carried out according to the manufacturer's instructions. Images of hybridized microarrays were acquired with a DNA microarray scanner (Agilent G2505B) and features were extracted using the Agilent Feature Extraction image analysis software (AFE) version A.10.7.3.1 with default protocols and settings. The AFE algorithm generates a single intensity measure for each microRNA, referred to as the total gene signal (TGS), which was used for further data analyses using the GeneSpring GX software package version 12.6.1. AFE-TGS were normalized by the quantile method. Subsequently, data were filtered on normalized expression values. Only entities where at least 2 out of 8 samples had values within the selected cutoff (75th-100th percentile) were further included in the data analysis process. A pairwise comparison of measured miRNA levels in obese versus non-obese mice, respectively, was performed. We conducted moderated t-test, unpaired, assuming equal variances using GeneSpring GX software package version 12.2.1. The p-values were adjusted for multiple testing according to Benjamini and Hochberg [FDR]34 and results were considered statistically significant at adjusted p-values below 0.05. Furthermore, only miRNAs with fold change ≥ 1.5 in the microarray analyses were considered worthy of more in-depth analyses.

3'UTR luciferase reporter assays. The 3'UTR-*Sirt7* Gaussia luciferase reporter construct, the 3'UTR-*TBX3* Gaussia luciferase reporter construct, and a control 3'UTR-reporter construct (all from Genecopoeia) were transfected into HEK293T cells using Lipofectamine (Invitrogen). In addition, we employed mutant 3'UTR-*Sirt7* Gaussia luciferase reporter constructs (CS-MMIT039823-MTO Mouse Sirt7 3'UTR Mutation). Co-transfection was performed with double-stranded miR-93 mimic (100nM) or control (Sigma). In some experiments, 20 % murine plasma from WT or miR-KO mice was used instead

of FCS. In addition, a Renilla Luciferase reporter construct was used as a transfection efficiency control for normalization. Secreted Gaussia luciferase activity was measured using the Secrete-Pair® Dual Luminescence Assay Kit (Genecopoeia). Renilla luciferase activity was measured using the Dual-Luciferase® Reporter Assay System (Promega). In both cases, luciferase activity was measured according to manufacturer's instructions and plotted as a percentage of the mock transfection.

Western Blot Analysis. Cells were harvested in RIPA buffer (Sigma) supplemented with a protease inhibitor cocktail (Roche Applied Science, Indianapolis, IN). 50µg of protein was resolved by SDS-PAGE and transferred to PVDF membranes (Amersham Pharmacia, Piscataway, NJ). Membranes were sequentially blocked with 1x TBS containing 5% BSA (w/v), and 0.1% Tween20 (v/v), incubated with antibodies against human SIRT7 (NB110-81746, Novus Biologicals; rabbit polyclonal, 1:200), mouse SIRT7 (Cell Signaling, rabbit mAb, clone D3K5A, product number #5360, 1:2,000 in 3% milk in TBS and 0.1% Tween20), GAPDH (ab8245, Abcam), ADIPONECTIN (abcam, ab22554; mouse antibody, 1:1,000), C/EBPa (2295, Cell Signaling; rabbit polyclonal, 1:1,000), PPARg (2435, Cell Signaling; rabbit polyclonal, diluted 1:1,000), and LEPTIN (ab16227, abcam; rabbit polyclonal, 1:1000) overnight at 4ºC, washed 3 times with 1x TBS containing 0.1% Tween 20 (v/v), incubated with horseradish peroxidase-conjugated secondary antibodies (Sigma), and washed again to remove unbound antibody. Bound antibody complexes were detected with SuperSignal chemiluminescent substrate (Amersham, Barcelona, Spain).

Immunostaining. Cells were seeded on chamber slides, fixed in 4% paraformaldehyde for 10 min and stained for FABP4 or SIRT7. Following several washes with PBS-T (PBS with 0.1 % Triton-X) and blocking with 0.1% bovine serum albumin in PBS-T, cells were incubated with FABP4 antibody (AF1443, R&D; goat polyclonal, 5µg/ml) or Sirt7 antibody (Novus Biologicals, NB110-81746: 1:20 in PBS-T) for 2 hours at RT, followed by visualization by secondary anti-goat Alexafluor 647 or 555 (Invitrogen) for FABP4 or by secondary anti-rabbit Alexafluor 488 (Invitrogen) for SIRT7. Nuclei were counterstained with DAPI prior to analysis using a Leica SP5 confocal microscope. Images were analyzed by ImageJ. In case of LipidTOX (Lifetechnologies; 1:1000 in PBS) lipid stainings in combination with

the nuclear transcription factor C/EBPa (2295, Cell Signaling; rabbit polyclonal, 1:50), cells were washed with PBS and only incubated for 20 min in PBS-T to minimize lipid destruction by Triton-X, while providing permeabilization for the C/EBPa staining. Visualization of C/EBPa staining was performed by secondary anti-rabbit Alexafluor 555 (Invitrogen) for 30 min. For tissue staining of frozen sections, sections were fixed in 4% paraformaldehyde for 10 min, followed by staining with LipidTOX for 10 min, or staining with ADIPONECTIN (abcam, ab22554; mouse antibody, 1:500) and GLUT-4 (Sigma, G4173; rabbit polyclonal, 1:150) for 30 min. Visualization was performed by secondary anti-mouse Alexafluor 647 or 555 (Invitrogen) for ADIPONECTIN or by secondary anti-rabbit Alexafluor 555 (Invitrogen) for GLUT-4 followed by DAPI staining.

Immunohistochemistry. Adipose tissue was harvested and fixed in 10% neutral buffered formalin then paraffin embedded. Sections were cut (2.5 μM) and immunohistochemical analysis was carried using the Ventana Discovery XT system (Roche). Sections were deparaffinized, hydrated, and loaded on the Discovery XT. Antigen retrieval was performed using citrate buffer solution. Endogenous peroxidases were quenched using H_2O_2 reagent (Ventana). Primary antibodies SIRT7 (Novus Biologicals, rabbit polyclonal, diluted 1:75) and PPARg (2435, Cell Signaling; rabbit polyclonal, diluted 1:300) were incubated for 20 min with the sections and then detected using an anti-rabbit secondary antibody and the ChromaMap DAB detection kit (Ventana). Tissues were counterstained with hematoxylin. Image analysis was carried out using Pannoramic viewer software (3DHISTECH).

Constructs for knockdown. To construct the lentiviral vectors carrying shRNA targeting human SIRT7, a forward and a reverse oligonucleotide for the shRNA was designed, in order to reconstitute the shRNAs through an hybridization PCR and introduce restriction sites at the 5' and 3' of the shRNA for posterior cloning. The oligonucleotides are shown in Table 2. The shRNAs were cloned in the lentiviral vector pLVX-shRNA2 from Clontech, under the control of the U6 promoter and with zsGreen as a transduction control. Replication-incompetent lentiviral particles were produced by calcium-phosphate transfection of HEK293T cells using the packaging plasmids pMD.2G (VSV-G) and pPAX2, as well as either one of the shRNA plasmids as shuttle vectors. The medium was replaced for fresh DMEM complete 6 h after

transfection, and 48h afterwards the medium was collected, cleared by low-speed centrifugation, filtered through 0.45μm pore size PVDF filters, and stored in aliquots at -80ºC.

Oligonucleotides for the production of shRNA against human SIRT7.

SIRT7.4 FW	5'GATCCACCGGGAACGGAACTCGGGTTATTGTTAGGTACCATAG CAATAACCCGAGTTCCGTTCTTTTG 3'
SIRT7.4 RV	5'AATTCAAAAGAACGGAACTCGGGTTATTGCTATGGTACCTAAC AATAACCCGAGTTCCGTTCCCGGTG 3'

To construct the lentiviral vectors carrying shRNAs targeting mouse *Tbx3*, a retroviral vector with the shRNAs 3579 and REN (control) was ordered from Mirimus. The shRNAs were subcloned using EcoRI and XhoI in the lentiviral SGEP vector also from Mirimus, a miR30-improved (miR-E) vector with GFP and shRNA driven-expression from the SFFV promoter. The sequences of the miR-E with the shRNAs are shown in Table 3. Replication-incompetent lentiviral particles were produced by calcium-phosphate transfection of HEK293T cells using the packaging plasmids pMD.2G (VSV-G) and pPAX2, as well as either one of the shRNA plasmids as shuttle vectors. The medium was replaced for fresh DMEM complete 6 h after transfection, and 48 h afterwards the medium was collected, cleared by low-speed centrifugation, filtered through 0.45 μm pore-size PVDF filters, and ultracentrifuged for 2 h at 20,000 rpm (4ºC). The pellet was then resuspended overnight at 4ºC with 300μl of NaCl 0.9%, and the viral concentrate was stored in aliquots at -80ºC.

Sequences of the miR-E + shRNAs against murine Tbx3.

miR-E + 3579	5'GAAGGCTCGAGAAGGTATATTGCTGTTGACAGTGAGCGAAGTGCACTT TGTTAGATGTAATAGTGAAGCCACAGATGTATTACATCTAACAAAGTGC ACTGTGCCTACTGCCTCGGACTTCAAGGGGCTAGAATTCGAGCA 3'
miR-E + REN	5'GAAGGCTCGAGAAGGTATATTGCTGTTGACAGTGAGCGCAGGAATTA TAATGCTTATCTATAGTGAAGCCACAGATGTATAGATAAGCATTATAAT TCCTATGCCTACTGCCTCGGACTTCAAGGGGCTAGAATTCGAGCA 3'

Statistical analysis. Results are expressed as the means ± SEM. Statistical analyses were performed with SPSS 22.0 (San Diego, CA) comparing continuous variables by non-parametrical Mann Whitney U and Kruskall-Wallis tests, and Chi-squared tests for categorical data. Significance is given as $p<0.05$.

3. SUPPLEMENTAL REFERENCES

Aicher, A., and Heeschen, C. (2007). Nonbone marrow-derived endothelial progenitor cells: what is their exact location? Circulation research 101, e102.

Aicher, A., Rentsch, M., Sasaki, K., Ellwart, J.W., Fändrich, F., Siebert, R., Cooke, J.P., Dimmeler, S., and Heeschen, C. (2007). Nonbone marrow-derived circulating progenitor cells contribute to postnatal neovascularization following tissue ischemia. Circulation research 100, 581-589.

Armamento-Villareal, R., Sheikh, S., Nawaz, A., Napoli, N., Mueller, C., Halstead, L.R., Brodt, M.D., Silva, M.J., Galbiati, E., Caruso, P.L., Civelli, M., and Civitelli, R. (2005). A new selective estrogen receptor modulator, CHF 4227.01, preserves bone mass and microarchitecture in ovariectomized rats. J Bone Miner Res 20, 2178-2188.

Berry, R., and Rodeheffer, M.S. (2013). Characterization of the adipocyte cellular lineage in vivo. Nat Cell Biol 15, 302-308.

Cole, J.H., Dowthwaite, J.N., Scerpella, T.A., and van der Meulen, M.C. (2009). Correcting fan-beam magnification in clinical densitometry scans of growing subjects. J Clin Densitom 12, 322-329.

Frank, D.U., Carter, K.L., Thomas, K.R., Burr, R.M., Bakker, M.L., Coetzee, W.A., Tristani-Firouzi, M., Bamshad, M.J., Christoffels, V.M., and Moon, A.M. (2012). Lethal arrhythmias in Tbx3-deficient mice reveal extreme dosage sensitivity of cardiac conduction system function and homeostasis. Proc Natl Acad Sci U S A 109, E154-163.

Galarraga, M., Campion, J., Munoz-Barrutia, A., Boque, N., Moreno, H., Martinez, J.A., Milagro, F., and Ortiz-de-Solorzano, C. (2012). Adiposoft: automated software for the analysis of white adipose tissue cellularity in histological sections. J Lipid Res 53, 2791-2796.

Gregoire, F.M., Smas, C.M., and Sul, H.S. (1998). Understanding adipocyte differentiation. Physiol Rev 78, 783-809.

Tomayko, M.M., and Reynolds, C.P. (1989). Determination of subcutaneous tumor size in athymic (nude) mice. Cancer Chemother Pharmacol 24, 148-154.